JACS
JOURNAL OF THE AMERICAN CHEMICAL SOCIETY
Article
pubs.acs.org/JACS

Combination of Small Molecule Prodrug and Nanodrug Delivery: Amphiphilic Drug–Drug Conjugate for Cancer Therapy

Ping Huang,[†] Dali Wang,[†] Yue Su,[†] Wei Huang,[†] Yongfeng Zhou,[†] Daxiang Cui,[‡] Xinyuan Zhu,*[,†] and Deyue Yan*[,†]

[†]School of Chemistry and Chemical Engineering, State Key Laboratory of Metal Matrix Composites, and [‡]Department of Bio-Nano Science and Engineering, Institute of Micro/Nano Science and Technology, Shanghai Jiao Tong University, 800 Dongchuan Road, Shanghai 200240, P. R. China

Supporting Information

ABSTRACT: All drugs for cancer therapy face several transportation barriers on their tortuous journey to the action sites. To overcome these barriers, an effective drug delivery system for cancer therapy is imperative. Here, we develop a drug self-delivery system for cancer therapy, in which anticancer drugs can be delivered by themselves without any carriers. To demonstrate this unique approach, an amphiphilic drug–drug conjugate (ADDC) has been synthesized from the hydrophilic anticancer drug irinotecan (Ir) and the hydrophobic anticancer drug chlorambucil (Cb) via a hydrolyzable ester linkage. The amphiphilic Ir–Cb conjugate self-assembles into nanoparticles in water and exhibits longer blood retention half-life compared with the free drugs, which facilitates the accumulation of drugs in tumor tissues and promotes their cellular uptake. A benefit of the nanoscale characteristics of the Ir–Cb ADDC nanoparticles is that the multidrug resistance (MDR) of tumor cells can be overcome efficiently. After cellular internalization, the ester bond between hydrophilic and hydrophobic drugs undergoes hydrolysis to release free Ir and Cb, resulting in an excellent anticancer activity in vitro and in vivo.

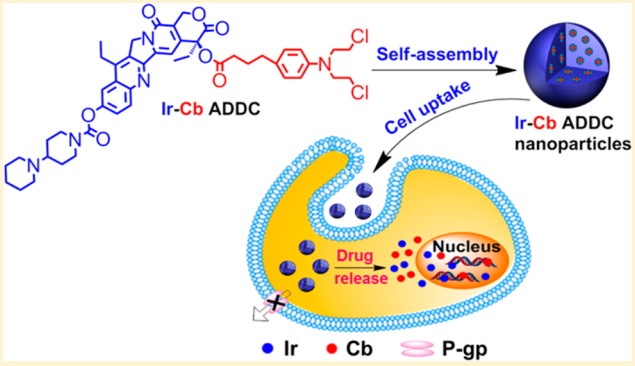

INTRODUCTION

Cancer is the leading disease of mortality in many countries of the world.[1] Therefore, how to fight against cancer is a great challenge for modern science and technology. Among various cancer treatments, chemotherapy is an indispensable choice for most cancer cases because of its high efficiency. Unfortunately, because of the small molecular size of free anticancer drugs, conventional chemotherapy suffers from several limitations including poor bioavailability, rapid blood/renal clearance, nonspecific selectivity, low accumulation in tumors, severe multidrug resistence (MDR), and adverse side effects for healthy tissues. To address these limitations, some nanovehicles[2−5] including water-soluble polymers,[6−11] liposomes,[12−14] vesicles,[15,16] polymeric nanoparticles,[17−19] and inorganic materials[20,21] have been used as drug carriers. With the help of these nanovehicles, drugs can be delivered to the action sites of a body via physical entrapment or chemical conjugation,[22−24] demonstrating better therapeutic efficacy against tumors and fewer side effects over free drugs.[25−27] However, almost all carriers have no therapeutic efficacy by themselves. Even worse, a lot of carriers with low drug loading capacity[28,29] may cause side-effects to kidneys and other organs in the course of degradation, metabolism, and excretion, such as high toxicity and serious inflammation.

Recently, scientists reported a new concept of directly conjugating hydrophobic drugs with small organic molecules to form nanodrug delivery systems. For example, Cui and co-workers constructed self-assembling drug amphiphiles by conjugating hydrophobic anticancer drugs to a short peptide segment.[30,31] This system could control both the self-assembled nanostructures and the drug loading content effectively. Shen and co-workers reported direct conjugation of a hydrophobic anticancer drug to a short oligomer ethylene glycol.[32] The resulting prodrug could self-assemble into a nanocapsule with high drug loading. Importantly, these small molecule prodrug-based delivery systems could remarkably enhance the drug loading capacity and improve cancer therapeutic efficacy. However, carriers are still indispensable in these small molecule prodrug delivery systems. It can be imagined that if the anticancer drugs could exhibit nanoscale characteristics by themselves without the help of nanovehicles, a promising drug self-delivery system integrating both the advantages of free drugs and nanocarriers could be expected. Aiming at this goal, we put forward a new ADDC concept and developed a novel self-delivery system of anticancer drugs in this work.

Received: May 24, 2014
Published: July 31, 2014

dx.doi.org/10.1021/ja505212y | J. Am. Chem. Soc. 2014, 136, 11748−11756

As a proof-of-concept, we describe here the novel ADDC strategy in Figure 1. The conjugate consists of a water-soluble

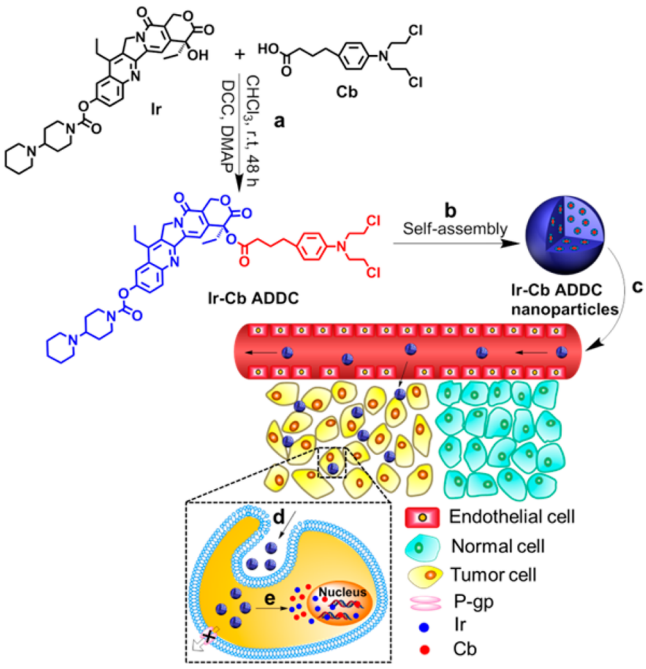

Figure 1. Schematic diagram of amphiphilic drug–drug conjugate (ADDC) from fabrication, self-assembly to self-delivery. (a) Synthesis of Ir–Cb ADDC through esterification in DCC/DMAP-catalyzed system. (b) The Ir–Cb ADDC self-assembles into nanoparticles in water. (c) Passive tumor targeting is achieved by the advantage of the EPR effect, which facilitates the Ir–Cb ADDC nanoparticles to access tumors by way of their leaky vasculature. (d) The Ir–Cb ADDC nanoparticles enter tumor cells by endocytosis. (e) Ir and Cb are released by the cleavage of the ester bond in tumor cells and then diffuse into nucleus.

anticancer drug Ir and a water-insoluble anticancer drug Cb (Figure 1a). Ir is a water-soluble derivative of camptothecin and a potent DNA topoisomerase I inhibitor in cancer cells,[33] which induces the death of tumor cells through DNA damage and transcription inhibition;[34] while Cb is one of water-insoluble DNA-alkylating anticancer drugs. Both Ir and Cb have been approved by the Food and Drug Administration (FDA). Ascribing to its amphiphilic structure, the Ir–Cb ADDC can self-assemble into nanoparticles in water to deliver themselves into tumor tissues possibly by passive accumulation via enhanced permeability and retention (EPR) effect[35,36] (Figure 1b,c). After the cellular internalization of Ir–Cb ADDC nanoparticles, both free Ir and Cb can be released to kill the cancer cells owing to the hydrolysis of the ester bond in the tumor cells (Figure 1d,e).

RESULTS AND DISCUSSION

Synthesis and Self-Assembly of Ir–Cb ADDC. The amphiphilic Ir–Cb conjugate was synthesized by esterification using DCC/DMAP (DCC, dicyclohexylcarbodiimide; DMAP, 4-dimethylamino-pyridine) as shown in Figure 1a, and the details are described in the Supporting Information. The chemical structure of Ir–Cb ADDC was confirmed by ^{1}H and ^{13}C nuclear magnetic resonance spectroscopy (^{1}H NMR, ^{13}C NMR) as shown in Figure 2a,b. Compared with the ^{1}H NMR spectrum of Ir in Figure 2a, the peak at 4.16 ppm (1) related to the hydroxyl proton disappears completely, and the two proton signals at 7.64 ppm (2) belonging to the pyridone ring and 1.87 ppm (3) attributed to the methylene (CH_3CH_2–, lactonic ring) of Ir shift to 7.17 ppm (2′) and 2.15 ppm (3′) in the ^{1}H NMR spectrum of the Ir–Cb conjugate. The proton shift of the pyridone moiety can be ascribed to strong π–π stacking after esterification. The proton signal at 2.13 ppm (4) corresponding to the methylene (–CH_2COOH) of Cb shifts to 2.28 ppm (4′) in the ^{1}H NMR spectrum of the Ir–Cb conjugate. In addition, as compared with the ^{13}C NMR spectrum of Cb in Figure 2b, the carbon signal at 180.37 ppm corresponding to the terminal COOH (1) of Cb disappears, and a new peak appears at 172.73 ppm (1′) corresponding to the –COO– group in the ^{13}C NMR spectrum of the Ir–Cb conjugate. Moreover, the carbon signal at 174.06 ppm (2) corresponding to –OCO– (lactonic ring) and 73.06 ppm (3) corresponding to HO–*C*CO– (lactonic ring) of Ir shift to 167.79 ppm (2′) and 75.96 ppm (3′) in the ^{13}C NMR spectrum of the Ir–Cb conjugate. The purity and molecular weight of Ir–Cb ADDC were further characterized by using liquid chromatography (LC) and mass spectrometry (MS) techniques (Supporting Information Figure S1). The Ir–Cb ADDC was also characterized by Fourier transform infrared spectroscopy (FTIR), ultraviolet–visible spectrophotometer (UV–vis), and fluorescence spectroscopy (Supporting Information Figures S2–S4). All experimental results demonstrate that Ir–Cb ADDC was synthesized successfully.

The inherent amphiphilicity of the Ir–Cb ADDC provides an opportunity for itself to self-assemble into nanoparticles in water. To determine the size and morphology of the self-assembled nanoparticles, a dimethyl sulfoxide (DMSO) solution of the Ir–Cb ADDC was added dropwise into water, followed by dialysis against water to remove DMSO. A stable and bluish solution with the final Ir–Cb conjugate concentration of 0.5 mg mL^{-1} was obtained. Figure 2c gives the dynamic light scattering (DLS) curve of Ir–Cb ADDC aqueous solution with a concentration of 0.5 mg mL^{-1}, indicating the formation of aggregates with a narrow unimodal distribution and an average hydrodynamic diameter of approximate 88.3 nm. The surface charge of the Ir–Cb ADDC solution was also investigated by DLS. The result shows that the value of zeta-potential is positive (+3.4) in phosphate buffer solution (PBS) (pH 7.4). The morphology of the aggregates was observed by transmission electron microscopy (TEM). The TEM image in Figure 2d shows the spherical nanoparticles with an average size of approximate 75.7 nm. This size is slightly smaller than that measured by DLS due to the shrinkage of nanoparticles in a drying state during TEM sample preparation. The inset of Figure 2d presents a typical enlarged TEM image of one nanoparticle, which clearly indicates that the nanoparticle consists of a lot of small spherical domains. These small domains are around 3.4 nm according to the statistical analysis of 50 samples, which supports that the small domains are conventional micelles self-assembled from Ir–Cb ADDCs since each ADDC is around 2 nm in size through simulations. Thus, the as-prepared nanoparticles are formed through the secondary aggregation of small micelles from ADDCs, which is similar to the small micelle aggregate (SMA) mechanism[37,38] or multicompartment micelle mechanism.[39] The detailed self-assembly mechanism is given in Supporting Information Figure S5. The DLS measurements at different time intervals demonstrated that the stability of Ir–Cb ADDC nanoparticles

dx.doi.org/10.1021/ja505212y | J. Am. Chem. Soc. 2014, 136, 11748–11756

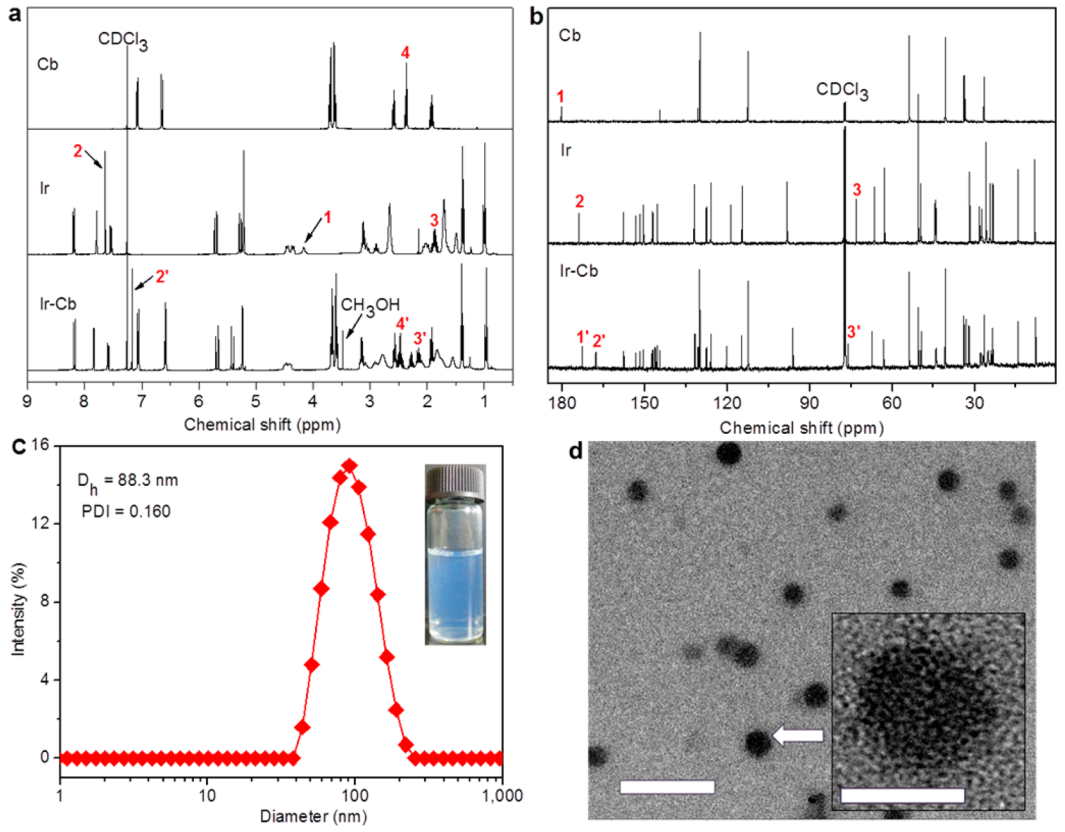

Figure 2. Chemical characterization of Ir−Cb ADDC and its self-assembled nanoparticles. (a) ^{1}H NMR and (b) ^{13}C NMR spectra of Cb, Ir, and Ir−Cb ADDC in $CDCl_3$. (c) DLS curve of Ir−Cb ADDC nanoparticles shows the diameter distribution of the nanoparticles, the polydispersity index (PDI = 0.160), and the average size (D_h = 88.3 nm). Inset: a digital photograph of Ir−Cb ADDC nanoparticle solution, exhibiting a stable, transparent bluish solution. (d) TEM image of Ir−Cb ADDC nanoparticles. Inset: the amplified image of a nanoparticle. Scale bars: 200 nm (d), 50 nm (inset).

was high enough for long storage (Supporting Information Figure S6).

To investigate the self-assembly behavior of Ir−Cb ADDC in water, the critical aggregation concentration (CAC) was measured by using pyrene as a fluorescent probe. I_1 and I_3 are the emission intensities of the first and third bands in the fluorescence spectrum of pyrene respectively, which are labeled as 1 and 3. The emission intensity ratio of I_3/I_1 is very sensitive to the polarity of the medium surrounding pyrene molecules.[40] The higher is polarity of the medium, the lower is the intensity ratio. The relationship of the I_3/I_1 ratio with the Ir−Cb ADDC concentration is present in Supporting Information Figure S7. At low Ir−Cb ADDC concentration, the I_3/I_1 value remains nearly unchanged, indicating the characteristics of pyrene in the water environment. With increasing Ir−Cb ADDC concentration, the ratio of I_3/I_1 starts to increase dramatically and reaches the characteristic level of pyrene in a hydrophobic environment at a certain Ir−Cb ADDC concentration. According to the inflection of the curve, the CAC value of the Ir−Cb ADDC is about 7 μg mL^{-1}.

The in vitro release behavior of Ir−Cb ADDC nanoparticles was evaluated by dialysis in PBS (pH 7.4) containing (or not) 10% FBS and PBS (pH 5.0) at 37 °C. The cumulative release curves in Supporting Information Figure S8 show that the concentration of released Ir is low in PBS (pH 7.4) containing 10% FBS (or not), suggesting the good stability of Ir−Cb ADDC nanoparticles under physiological conditions and in the presence of serum. Meanwhile, the time-dependent changes in hydrodynamic diameter of Ir−Cb ADDC nanoparticles were measured by DLS, which further confirms the high stability of Ir−Cb ADDC nanoparticles in serum (Supporting Information Figure S9). However, at a weakly acidic environment (pH 5.0), the hydrolysis of Ir−Cb ADDC is accelerated and more free Ir and Cb drugs are released. The hydrodynamic diameter of Ir−Cb ADDC nanoparticles significantly changes with increasing time at pH 5.0, which may result from the degradation of the ester bond (Supporting Information Figure S10).

To further confirm whether the Ir−Cb ADDC was converted into free Ir and Cb through ester degradation in cells, we carried out the study of intracellular degradation. After the MCF-7 cancer cells (a human breast adenocarcinoma cell line) were incubated with Ir−Cb ADDC nanoparticles for 6 h, the cellular extracts were measured by a liquid chromatography−mass spectroscopy (LC−MS) technique. The mixed standard with Cb, Ir, and Ir−Cb was used as a control. The LC−MS data of cellular extracts (Supporting Information Figure S12) verify the existence of free Cb and Ir together with Ir−Cb after incubation with Ir−Cb ADDC nanoparticles by comparing those of the mixed standards (Supporting Information Figure S11). The intracellular degradation studies demonstrate that the ester bond between hydrophilic and hydrophobic drugs is hydrolyzed to release both free Ir and Cb within cancer cells.

In Vitro Studies of Ir−Cb ADDC Nanoparticles. Ir emits blue fluorescence under UV-lamp irradiation. The fluorescence spectra of Ir and Ir−Cb ADDC in acetonitrile are shown in the Supporting Information Figure S4a. The fluorescence spectros-

dx.doi.org/10.1021/ja505212y | J. Am. Chem. Soc. 2014, 136, 11748−11756

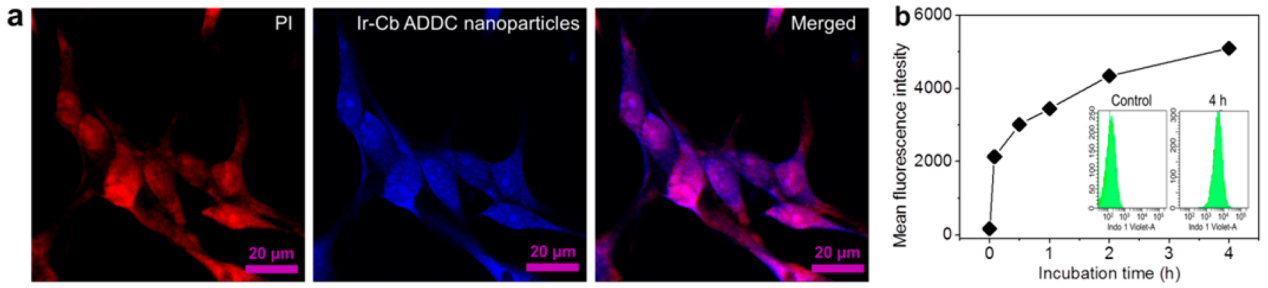

Figure 3. Cellular uptake of Ir−Cb ADDC nanoparticles by MCF-7 cells. (a) CLSM photos of MCF-7 cells incubated with Ir−Cb ADDC nanoparticles for 4 h. Cell nuclei are stained with PI. (b) Time-dependent profiles of ADDC nanoparticles fluorescence intensity in the MCF-7 cells by flow cytometry analysis. Insert: representative flow cytometry histogram profiles of MCF-7 cells cultured with Ir−Cb nanoparticles for 4 h, the untreated cells are used as a control.

copy studies (Supporting Information Figure S4b) show that the self-assembled Ir−Cb ADDC nanoparticles in water also emit strong blue fluorescence, suggesting that they can be used as probes for cell imaging. The cellular uptake of Ir−Cb ADDC nanoparticles was studied by confocal laser scanning microscopy (CLSM). MCF-7 cells were cultured with Ir−Cb ADDC nanoparticles for 4 h before observation. The nuclei were stained for 15 min with propidium iodide (PI), and the prepared cells were observed using a LEICA TCS SP8. As shown in Figure 3a, the blue fluorescence of Ir−Cb ADDC nanoparticles is in both cytoplasm and nuclei according to the merged image. The results demonstrate that Ir−Cb ADDC nanoparticles could be internalized by the cells. The cellular uptake of Ir−Cb ADDC nanoparticles was further confirmed by flow cytometric analysis. Figure 3b shows that the fluorescence intensity of cells increases with the incubation time, which can be attributed to the cellular uptake of more and more Ir−Cb ADDC nanoparticles by MCF-7 cells.

The proliferation inhibition of Ir−Cb ADDC nanoparticles was evaluated against MCF-7 and HeLa (a human cervical carcinoma cell line) cancer cells, comparing with free Cb, Ir, and Ir/Cb mixture. The cells without any treatment were used as the control. As displayed in Figure 4a, the cytotoxicity to MCF-7 cancer cells of free Ir and Ir/Cb mixture is nearly the same but much higher than that of free Cb, probably due to the difficult uptake of hydrophobic Cb by tumor cells. The therapeutic efficacy of Ir−Cb ADDC is strongly dependent on drug concentration. If the drug concentration is lower than the CAC value, the antitumor activity of Ir−Cb ADDC is worse than that of free Ir and Ir/Cb mixture. When the concentration of Ir−Cb ADDC is higher than the CAC value, it shows much better anticancer efficiency than free Ir and Ir/Cb mixture. The higher anticancer efficacy suggests that the self-assembled Ir−Cb ADDC nanoparticles enter into tumor cells, and the released free Ir and Cb might play a synergistic action. The similar phenomenon is also found in other cancer cell lines such as HeLa cells (Figure 4b).

MDR is one major cause of clinical treatment failure for cancer therapy, especially for small-molecule anticancer drugs. One of the main mechanisms of MDR is drug efflux mediated by transporters such as P-glycoprotein (P-gp), which belongs to the ATP-binding cassette (ABC) family of membrane transporters. P-gp can use the energy from ATP-hydrolysis to pump free small-molecule anticancer drugs out of tumor cells, resulting in a reduction of the drug accumulation in tumor cells.[41,42] Fortunately, the nanoparticles can bypass the P-gp efflux pump, accumulate themselves in cells, and deliver drugs into cytoplasm efficiently.[43,44] Hence, the Ir−Cb ADDC nanoparticles are expected to overcome the MDR of tumor cells. We studied the accumulation assay of free Ir and Ir−Cb ADDC nanoparticles using drug-sensitive MCF-7 cells and drug-resistant MCF-7/ADR cells. Owing to the low expression of P-gp, the accumulation of free Ir in MCF-7 cells is rather high and increases with incubation time. Contrarily, the accumulation of free Ir in MCF-7/ADR cells is extremely low due to MDR, which decreases to 1/50−1/60 compared with that in MCF-7 cells (Figure 4d). Interestingly, remarkable accumulation is observed in both MCF-7 cells and MCF-7/ADR cells when incubation with Ir−Cb ADDC nanoparticles for the same period. The amount of Ir−Cb conjugate in MCF-7/ADR cells is about 1/2 to that in MCF-7 cells (Figure 4e), which may be attributed to the high cellular internalization of Ir−Cb ADDC nanoparticles and efficient resistance to P-gp mediated drug efflux. If the cells were first treated with free Ir and Ir−Cb ADDC nanoparticles for 4 h and then incubated with fresh medium for various times, similar results were obtained, as shown in Supporting Information Figure S13.

To further confirm the anticancer efficiency of Ir−Cb ADDC nanoparticles on MDR tumor cells, we investigated the cytotoxicity of various drug formulations by methyl tetrazolium (MTT) assay (Figure 4c). In MCF-7/ADR cells, the half-maximal inhibitory concentration (IC_{50}) values of free Ir and Ir/Cb mixture (Figure 4c) are as high as 100 μM as the result of high overexpression of P-gp, which has ~20-fold resistance to Ir and Ir/Cb mixture by comparison to the MCF-7 (IC_{50}: 5 μM, Figure 4a, Table S1 in the Supporting Information). However, the IC_{50} (15 μM) of Ir−Cb ADDC nanoparticles in MCF-7/ADR cells is not significantly different from that (13 μM) in MCF-7 cells (Figure 4a,c). These observations demonstrate that the Ir−Cb ADDC nanoparticles can overcome the MDR of tumor cells.

It is well-known that most small-molecule anticancer drugs generally kill tumor cells by activating apoptosis. Here, the FITC-Annexin V/propidium iodide (PI) method was used to determine whether the death of cancer cells incubating with Ir−Cb ADDC nanoparticles was induced by apoptosis. MCF-7 cells were first incubated with Cb, Ir, Ir/Cb mixture, and Ir−Cb ADDC nanoparticles at the same concentration (30 μM) for 24 h and then subjected to FITC-Annexin V/PI staining. The untreated cells were used as control. The flow cytometry analysis shows that the ratio of apoptosis cells is 18.02%, 25.10%, or 26.03% induced by Cb, Ir, or Ir/Cb mixture, and increases to 76.87% if incubation with Ir−Cb ADDC nanoparticles (Figure 4f). In comparison with other formulations, the Ir−Cb ADDC nanoparticles promote a much higher apoptotic rate of MCF-7 cells with the same dose.

dx.doi.org/10.1021/ja505212y | J. Am. Chem. Soc. 2014, 136, 11748−11756

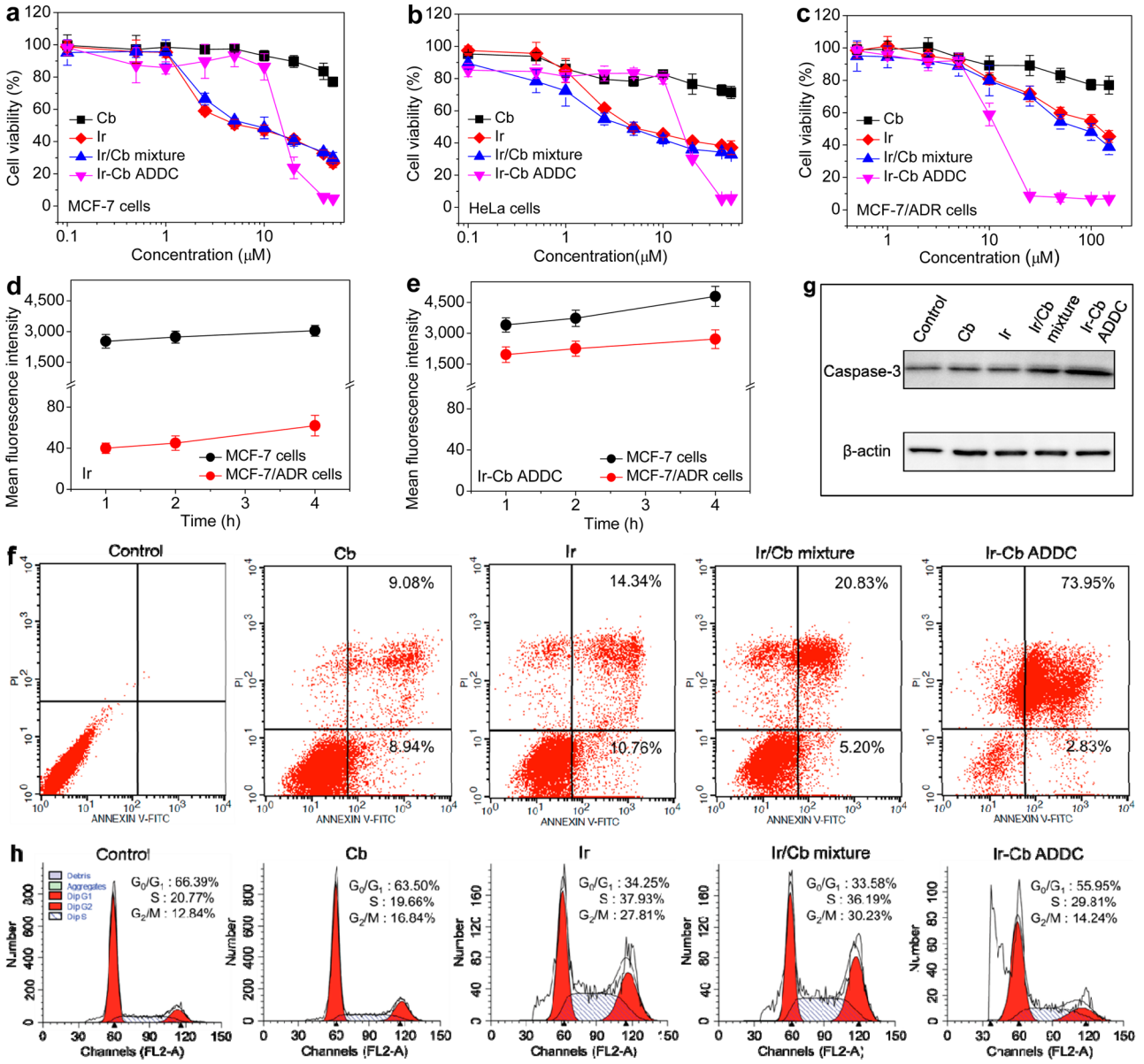

Figure 4. Effect of Ir−Cb ADDC nanoparticles on cancer cell growth, cell cycle, and cell apoptosis-related protein expression in vitro. (a,b,c) In vitro cytotoxicity of Cb, Ir, Ir/Cb mixture, and Ir−Cb ADDC nanoparticles to MCF-7 cells (a), HeLa cells (b), and MCF-7/ADR cells (c) determined by MTT assay. The data are presented as average ± standard error (n = 6). (d) The accumulation of free Ir in MCF-7 cells and MCF-7/ADR cells after incubation with Ir for different time. (e) The accumulation of Ir−Cb ADDC in MCF-7 cells and MCF-7/ADR cells after incubation with Ir−Cb ADDC nanoparticles for different time. (f) Flow cytometry analysis for apoptosis of MCF-7 cells induced by Cb, Ir, Ir/Cb mixture, and Ir−Cb ADDC nanoparticles at the same concentration of 30 μM for 24 h. Lower left, living cells; lower right, early apoptotic cells; upper right, late apoptotic cells; upper left, necrotic cells. Inserted numbers in the profiles indicate the percentage of the cells present in this area. (g) The expression levels of caspase-3 in MCF-7 cells induced by Cb, Ir, Ir/Cb mixture, and Ir−Cb ADDC nanoparticles at the same concentration (30 μM) for 24 h, determined by Western blot analysis. Cells untreated are used as a control, and β-actin is the loading control. Data represent three individual experiments. Each experiment group is repeated three times. (h) The cell cycle distribution histograms of MCF-7 cells treated with Cb, Ir, Ir/Cb mixture, and Ir−Cb ADDC nanoparticles at the same concentration of 30 μM for 24 h.

Caspases, as a family of intracellular cysteine-aspartyl proteases, play an essential role in apoptosis. Among them, caspase-3 has been considered as a key effector of cell apoptosis and identified as being activated in response to cytotoxic drugs.[45−47] To verify whether the caspase-3 was activated by Ir−Cb ADDC nanoparticles, the Western blot analysis was used to examine the expression of caspase-3 protein. First, MCF-7 cells were incubated with Cb, Ir, Ir/Cb mixture, and Ir−Cb ADDC nanoparticles at the same concentration for 24 h. The untreated MCF-7 cells were used as a negative control. The Western blot data reveal that caspase-3 protein expression is up-regulated slightly by Cb, Ir, and Ir/Cb mixture in comparison with untreated control, whereas the expression of caspase-3 protein is markedly enhanced by Ir−Cb ADDC nanoparticles (Figure 4g). These results clearly indicate that although caspase-3 can be activated by various formulations, the Ir−Cb ADDC nanoparticles are the most effective one to promote the activation of caspase-3.

We also assessed the effect of Ir−Cb ADDC nanoparticles on cell cycle by measuring DNA content with the help of flow

dx.doi.org/10.1021/ja505212y | J. Am. Chem. Soc. 2014, 136, 11748−11756

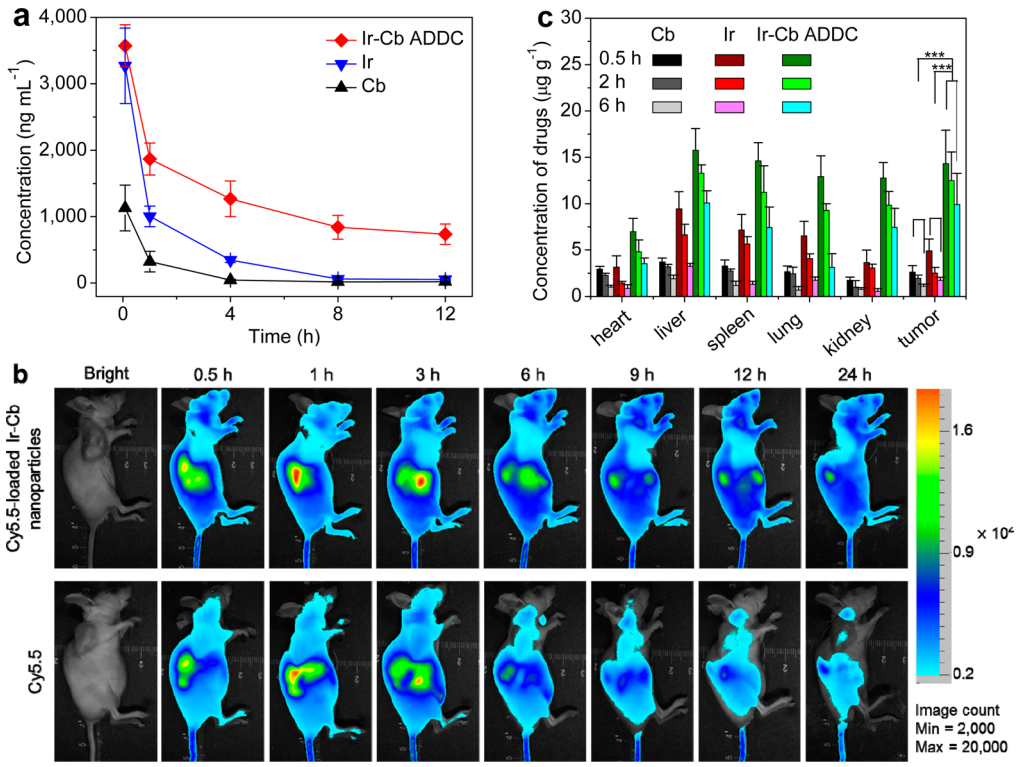

Figure 5. In vivo pharmacokinetics and biodistribution of Ir−Cb ADDC nanoparticles. (a) Representative plasma concentration−time profiles of free Cb, Ir, and Ir−Cb ADDC after i.v. injection into rats (a dose of 8 mg kg^{-1}). The data are presented as the average ± standard error (n = 4). (b) In vivo noninvasive NIRF images of time-dependent whole body imaging of MCF-7 tumor-bearing nude mice after intravenous injection of free Cy5.5 and Cy5.5-loaded Ir−Cb ADDC nanoparticles. (c) Tissue distribution of Cb, Ir, and Ir−Cb ADDC after intravenous injection of free Cb (3.5 mg kg^{-1}), Ir (6.7 mg kg^{-1}), and Ir−Cb ADDC nanoparticles (10 mg kg^{-1}) in nude mice. Data are presented as average ± standard error (n = 4), and the statistical significance level is ***P < 0.001.

cytometry. First, cells were treated with Cb, Ir, Ir/Cb mixture, and Ir−Cb ADDC nanoparticles for 24 h and then stained with PI. The results in Figure 4h show that cells treated with Cb exhibit a similar cell cycle to that of the control cells. However, the cell cycle is significantly changed after incubation with Ir and Ir/Cb mixture: the percentage of G_0/G_1 phase decreases to 34.25% and 33.58%, the percentage of G_2/M increases to 27.81% and 30.23%, while the percentage of S increases to 37.93% and 36.19%, respectively. When the cells are incubated with Ir−Cb ADDC nanoparticles, the cell cycle changes and shows an obvious sub-G_0/G_1 apoptotic phase. These results are consistent with apoptosis analysis.

Blood Retention Time and Biodistribution Studies. As compared to free small-molecule drugs, nanoparticles with a suitable size (<200 nm) usually show a longer retention time in the bloodstream.[48] To confirm this hypothesis, the pharmacokinetic study was undertaken by i.v. injection of the free Cb, Ir, and Ir−Cb ADDC nanoparticles to Sprague−Dawley (SD) rats (~200 g). Figure 5a gives the time profiles of the free Cb, Ir, and Ir−Cb ADDC nanoparticles in plasma. It can be seen that the Ir−Cb ADDC nanoparticles are retained at a higher concentration in the bloodstream up to 12 h, whereas the concentration of free Cb and Ir is only 1/20 of the Ir−Cb ADDC after 12 h in the bloodstream. As compared to that of free Cb and Ir, the longer blood retention time of Ir−Cb ADDC nanoparticles provides the possibility of enhanced drug accumulation in the tumor tissues.

To further evaluate the blood retention time of Ir−Cb ADDC nanoparticles, Cy5.5, a near-infrared fluorescence (NIRF) dye, was loaded in Ir−Cb ADDC nanoparticles to form Cy5.5-loaded Ir−Cb ADDC nanoparticles. The preparation method is described in the Supporting Information. Both DLS and TEM observations (Supporting Information Figures S14−S15) show that the size of Ir−Cb ADDC nanoparticles is almost unchanged after encapsulation with Cy5.5. Free Cy5.5 and Cy5.5-loaded Ir−Cb ADDC nanoparticles were intravenously injected via tail vein into MCF-7 tumor-bearing nude mice. Subsequently, the real-time imaging of Ir−Cb ADDC nanoparticles in the tumor-bearing mice was monitored over the course of 24 h (Figure 5b). Upon i.v. injection, the NIRF signals of free Cy5.5 in the whole body significantly increase to the strongest after 1 h, and then subsequently decrease from 1 to 6 h. After 24 h, the signals in the whole body are extremely weak, indicating that free Cy5.5 has been quickly cleared from the bloodstream. On the other hand, the NIRF signals of Cy5.5-loaded Ir−Cb ADDC nanoparticles in the whole body gradually increase up to 3 h. As compared to free Cy5.5, the Cy5.5-loaded Ir−Cb ADDC nanoparticles maintain higher NIRF intensity up to 24 h. The longer retention promotes the tumor accumulation of the nanoparticles.

Furthermore, to examine the amount of Ir−Cb ADDC in the tumors and other organs, the MCF-7 tumor-bearing mice were sacrificed after intravenous injection with different time intervals. The tumor-bearing mice treated with free Cb and Ir were used as controls. The biodistribution profiles show that a large amount of Ir−Cb ADDC accumulate in liver, spleen, kidney, lung, and tumor in the first 2 h. After 6 h postinjection, the content of Ir−Cb ADDC obviously decreases in kidney, spleen, and lung, whereas the downward trend in tumor and liver is slower (Figure 5c). The large accumulation of Ir−Cb

dx.doi.org/10.1021/ja505212y | J. Am. Chem. Soc. 2014, 136, 11748−11756

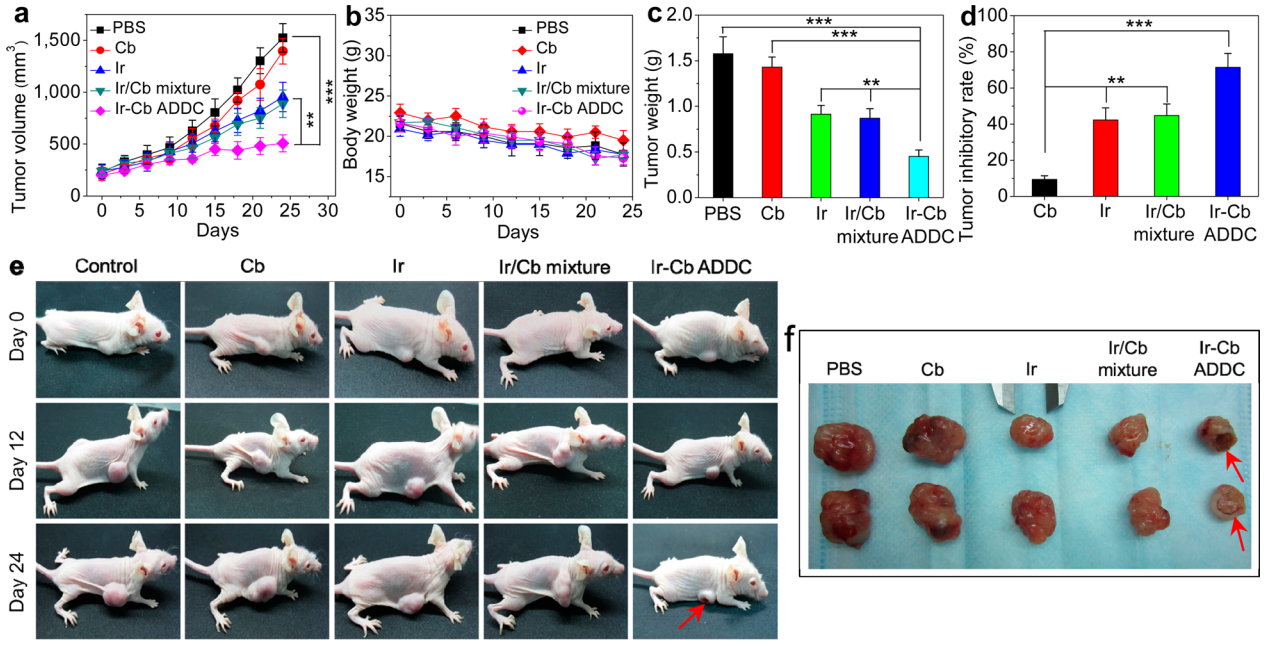

Figure 6. In vivo anticancer activity. (a) Changes of tumor volume after intravenous injection of PBS, Cb, Ir, Ir/Cb mixture, and Ir−Cb ADDC nanoparticles in MCF-7 tumor-bearing nude mice. (b) Body weight changes of MCF-7 tumor-bearing mice after treatment with PBS, Cb, Ir, Ir/Cb mixture, and Ir−Cb ADDC nanoparticles. (c) Mean weight of tumors separated from mice after different treatments. (d) The tumor inhibitory rate (TIR) after treatment with Cb, Ir, Ir/Cb mixture, and Ir−Cb ADDC nanoparticles in MCF-7 tumor-bearing nude mice. The TIR is calculated using the following equation: TIR(%) = 100 × (mean tumor weight of control group − mean tumor weight of experimental group)/mean tumor weight of control group. Data are represented as average ± standard error ($n = 6$). Statistical significance: $^{**}P < 0.005$; $^{***}P < 0.001$. (e) The mice are treated with different formulations and the tumor size is real-time monitored during the 24-day evaluation period. (f) Representative tumors separated from animals after intravenous injection of PBS, Cb, Ir, Ir/Cb mixture, and Ir−Cb ADDC nanoparticles.

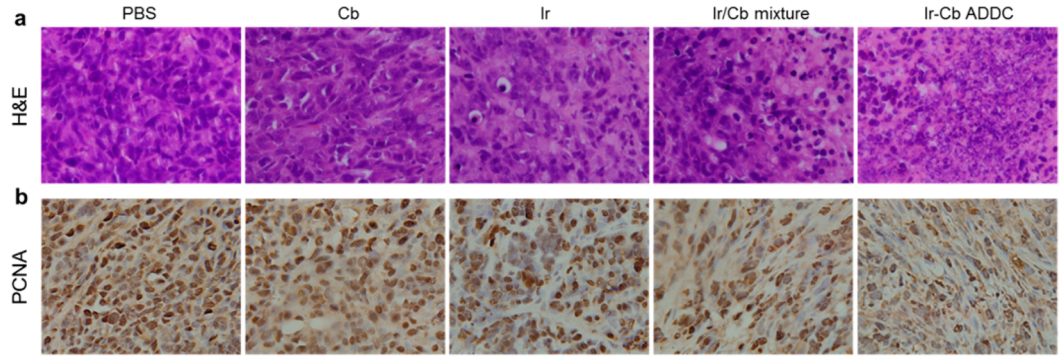

Figure 7. Immunohistochemical analysis of tumor tissues treated with various treatments. (a) Tumors are sectioned and stained with H&E. (b) Tumor sections are evaluated for PCNA expression using an antimouse PCNA antibody (magnification ×400).

ADDC nanoparticles in other organs can be due to the nanoscale characteristic of nanoparticles, which may result in a long-term toxicity. Compared to that of the Ir−Cb ADDC, the concentration of free Cb and Ir is remarkably lower in the tumor and other organs. Ir mainly accumulates in the liver, followed by spleen, lung, kidney, and heart up to 2 h. After 6 h, the Ir concentration in the spleen and lung decreases quickly. In contrast, Cb largely accumulates in the liver, followed by spleen, lung, heart, and kidney. These data indicate that Ir−Cb ADDC nanoparticles can be accumulated in tumors probably by passive targeting through the EPR effect.

In Vivo Antitumor Activity Studies of Ir−Cb ADDC Nanoparticles. To evaluate whether efficient accumulation and improved biodistribution results in the enhancement of therapeutic efficacy, MCF-7 tumor-bearing mice were intravenously injected with Cb, Ir, Ir/Cb mixture, Ir−Cb ADDC nanoparticles, and phosphate buffer solution (PBS) as control via the tail vein. Tumor volume and body weight of tumor-bearing mice were monitored every 3 days for 24 days. At the end of the experiments, the tumor volumes (Figure 6a) in mice treated with Ir−Cb ADDC nanoparticles were much smaller than the tumor volumes in mice treated with PBS, Cb, Ir and Ir/Cb mixture. Compared with that of the PBS group, the tumor volume after 24 days treatment is 91.60 ± 2.09% for Cb, 62.65 ± 5.26% for Ir, 58.31 ± 7.34% for Ir/Cb mixture, or 32.11 ± 3.07% for Ir−Cb ADDC nanoparticles, which shows that Ir−Cb ADDC nanoparticles procure predominant tumor growth inhibitory efficacy than Cb, Ir and Ir/Cb mixture. This therapeutic efficacy in our work is in line with the previous reports in camptothecin nanodrugs.[49,50] Meanwhile, no obvious change in efficacy is observed between Ir and Ir/Cb mixture groups. For the Cb formulation, no significantly therapeutic

dx.doi.org/10.1021/ja505212y | J. Am. Chem. Soc. 2014, 136, 11748−11756

efficacy is found. These observations are in accordance with the results of in vitro evaluations. In addition, the tumor volume of mice treated with Ir−Cb ADDC nanoparticles is much smaller than the tumor volume of mice treated with Cb, Ir, and Ir/Cb mixture, while there is about 15% loss of body weight for tumor-bearing mice treated with various formulations, illustrating a few side effects of Ir−Cb ADDC nanoparticles for tumor therapy (Figure 6b). After 24 days treatment, mice were sacrificed and tumors were dissected and photographed (Figure 6f). The tumor inhibitory rate (TIR) was calculated from tumor weight (Figure 6c). Compared with that of the PBS group, the TIR of Ir−Cb ADDC nanoparticles is 71.40 ± 7.75%, which is significantly higher than that of Cb (9.3 ± 2.10%), Ir (42.3 ± 6.63%), and Ir/Cb mixture (44.8 ± 6.31%) (Figure 6d). Interestingly, the tumor necrosis occurs after treatment with Ir−Cb ADDC nanoparticles (Figure 6e,f, red arrow). These results further demonstrate that the therapeutic efficacy of Ir−Cb ADDC nanoparticles is the highest in all of the therapeutic groups.

The immunohistochemical analysis was adopted to assess the different antitumor efficacy after treatment with various formulations. Histological examination of hematoxylin and eosin (H&E) stained tissue sections indicates obvious differences in tissue morphology between PBS and treated groups (Figure 7a). The tumor cells treated with PBS group are observed with large nucleus and spindle shape in the tumor tissues, determining a rapid tumor growth. A similar result is achieved from treatment of Cb. By contrast, the tumor cellularity,[51] as evaluated by average tumor cell numbers of each microscopic field, decreases significantly, and nuclear shrinkage and fragmentation are observed in the Ir, Ir/Cb, and Ir−Cb ADDC treated groups, especially for the Ir−Cb ADDC treated tumors. Meanwhile, a large necrotic area is observed in the Ir−Cb ADDC group. The proliferating cell nuclear antigen (PCNA) was used to analyze cell proliferation in the tumor tissues after treatment of various formulations. The results clearly indicate that the percentage of PCNA-positive (brown) tumor cells gradually decreases in the mice treated with various drug formulations compared with those of the PBS group (Figure 7b). However, the percentage of PCNA-positive tumor cells treated with Ir−Cb ADDC nanoparticles is the lowest one among the therapeutic groups, resulting from the tumor cell proliferation inhibition in MCF-7 tumor-bearing mice. Hence, both H&E and PCNA staining results confirm the superior in vivo antitumor efficacy of Ir−Cb ADDC nanoparticles.

CONCLUSIONS

Chemotherapy remains one of the major strategies for cancer treatment. Despite small-molecule chemotherapeutic drugs being extensively applied in clinic, they still face several formidable problems. First, most of the chemotherapeutic drugs such as Cb are hydrophobic, resulting in low solubility. Second, the retention time of small-molecule anticancer drugs in the bloodstream is short because of the elimination from the reticuloendothelial system (ERS), even for hydrophilic anticancer drugs including Ir, which leads to poor bioavailability of drugs. In the present work, our observation confirms that the drug concentration in the bloodstream is extremely low shortly after injection of free Ir and Cb. Third, the enrichment of drugs in the tumor site is difficult as a result of nontargeted chemotherapeutic drugs. Fourth, the MDR reduces the drug accumulation in tumor cells greatly and renders therapeutic failure. Owing to the existence of these insurmountable transportation barriers, neither hydrophilic chemotherapeutic drugs such as Ir nor hydrophobic ones such as Cb show satisfactory anticancer activity. By mixing hydrophilic Ir and hydrophobic Cb together, little improvement has been observed. Astonishingly, we find here that all of these annoying problems might be resolved by simple conjugation of a hydrophilic anticancer drug with a hydrophobic one through a biodegradable bond. Our experimental results have demonstrated that compared to FDA-approved free Ir, Cb, or Ir/Cb mixture, the Ir−Cb conjugate consisting of hydrophilic Ir and hydrophobic Cb through a hydrolyzable ester linkage exhibits a much better therapeutic effect.

The excellent therapeutic effect of the Ir−Cb conjugate can be attributed to molecular self-assembly. Benefiting from its amphiphilicity, the Ir−Cb conjugate self-assembles into ADDC nanoparticles with an average hydrodynamic diameter of 88.3 nm in water. Generally speaking, the nanoscale characteristics of particles are beneficial for escaping from the RES elimination. Our experimental data clarify that the Ir−Cb ADDC nanoparticles have much longer blood retention time than free Ir and Cb, which results in higher tumor accumulation of drugs. After the cellular internalization of Ir−Cb ADDC nanoparticles, the P-gp mediated drug efflux is efficiently avoided. All of these results show that the drugs can be self-delivered by themselves effectively without the help of any carriers. As we know, to achieve the nanoscale characteristics of drug delivery systems, various nanocarriers have been designed and prepared. However, the introduction of drug carriers causes several problems, such as low drug loading and poor quality control. Moreover, the degradation, metabolism, and excretion of these carriers may cause some side-effects to tissues and organs. Hence, FDA approval is difficult for most of the carriers, which limits their application in clinic. Different from these carrier-based drug delivery systems, the carrier-free Ir−Cb ADDC nanoparticles are composed of two anticancer drugs, in which most problems from carriers no longer exist. In the meantime, the Ir−Cb ADDC nanoparticles exhibit nanoscale advantages, increasing the accumulation of Ir−Cb conjugate in the tumor tissue. However, Ir−Cb ADDC nanoparticles still accumulate in other organs similar to conventional nanoparticles, which may cause a long-term toxicity. The problem can be derived from nanoparticles themselves, which is a universal phenomenon for nanomedicine. Our results demonstrate that the ester bond between hydrophilic Ir and hydrophobic Cb can be hydrolyzed to release the free Ir and Cb after cells being cultured with Ir−Cb ADDC nanoparticles. The released Ir and Cb kill cancer cells efficiently, leading to an excellent anticancer activity in vitro and in vivo.

In summary, we put forward a new concept, ADDC, and develop a novel self-delivery system of antitumor drugs for cancer therapy. The data in this study clearly show that the Ir−Cb ADDC can self-assemble into nanoparticles in an aqueous solution, leading to longer retention time than the corresponding free drugs in the bloodstream. The longer retention time facilitates the accumulation of anticancer drugs in tumor tissues and the subsequent cellular internalization. The nanoscale characteristics of Ir−Cb ADDC nanoparticles can circumvent the MDR of the tumor cells in chemotherapy, resulting in high intracellular drug concentration. After hydrolysis of the ADDC, the two released free anticancer drugs exert synergetic cytotoxicity to the tumor cells, exhibiting higher apoptotic rate and anticancer activity than the individual free drugs. These advantages of Ir−Cb ADDC nanoparticles result in a superior

anticancer efficacy in vivo. Overall, we believe that this drug self-delivery strategy based on self-assembly of amphiphilic drug−drug conjugate in the present study may open a new way for chemotherapy in cancer therapy and would eventually be applied in clinic for the treatment of varieties of tumors.

■ ASSOCIATED CONTENT

Supporting Information

Synthesis detail of Ir−Cb ADDC and FTIR, UV−vis and fluorescence characterization data for the ADDC; preparation of Ir−Cb ADDC nanoparticles; in vitro cell experiments; Western blot analysis; animals and tumor models; pharmacokinetics and biodistribution; in vivo anticancer activity and immunohistochemical analysis. This material is available free of charge via the Internet at http://pubs.acs.org.

■ AUTHOR INFORMATION

Corresponding Authors

dyyan@sjtu.edu.cn
xyzhu@sjtu.edu.cn

Notes

The authors declare no competing financial interest.

■ ACKNOWLEDGMENTS

The authors thank Na Zhu and Lei Feng (Instrumental Analysis Center of Shanghai Jiao Tong University) for UPLC-3Q and LC−MS assay and Bing Liu for in vivo experiments. We thank the National Basic Research Program (2013CB834506, 2012CB821500, 2011CB933101), the National Natural Science Foundation of China (91127047), and China National Funds for Distinguished Young Scientists (21025417) for financial support.

■ REFERENCES

(1) Ferlay, J.; Shin, H.-R.; Bray, F.; Forman, D.; Mathers, C.; Parkin, D. M. *J. Cancer* **2010**, *127*, 2893−2917.
(2) Park, J. H.; Lee, S.; Kim, J.-H.; Park, K.; Kim, K.; Kwon, I. C. *Prog. Polym. Sci.* **2008**, *33*, 113−137.
(3) Hubbell, J. A.; Chilkoti, A. *Science* **2012**, *337*, 303−305.
(4) Tong, R.; Cheng, J. *Polym. Rev.* **2007**, *47*, 345−381.
(5) Riehemann, K.; Schneider, S. W.; Luger, T. A.; Godin, B.; Ferrari, M.; Fuchs, H. *Angew. Chem., Int. Ed.* **2009**, *48*, 872−897.
(6) Fox, M. E.; Szoka, F. C.; Fréchet, J. M. J. *Acc. Chem. Res.* **2009**, *42*, 1141−1151.
(7) Lutz, J.-F.; Börner, H. G. *Prog. Polym. Sci.* **2008**, *33*, 1−39.
(8) Kiick, K. L. *Science* **2007**, *317*, 1182−1183.
(9) Lee, C. C.; MacKay, J. A.; Fréchet, J. M. J.; Szoka, F. C. *Nat. Biotechnol.* **2005**, *23*, 1517−1526.
(10) Zhou, Y.; Huang, W.; Liu, J.; Zhu, X.; Yan, D. *Adv. Mater.* **2010**, *22*, 4567−4590.
(11) Liu, J.; Pang, Y.; Huang, W.; Zhu, X.; Zhou, Y.; Yan, D. *Biomaterials* **2010**, *31*, 5643−5651.
(12) Lee, S.-M.; Chen, H. M.; Dettmer, C. M.; O'Halloran, T. V.; Nguyen, S. T. *J. Am. Chem. Soc.* **2007**, *129*, 15096−15097.
(13) Volodkin, D. V.; Skirtach, A. G.; Möhwald, H. *Angew. Chem., Int. Ed.* **2009**, *48*, 1807−1809.
(14) Linderoth, L.; Fristrup, P.; Hansen, M.; Melander, F.; Madsen, R.; Andresen, T. L.; Peters, G. H. *J. Am. Chem. Soc.* **2009**, *131*, 12193−12200.
(15) Holme, M. N.; Fedotenko, I. A.; Abegg, D.; Althaus, J.; Babel, L.; Favarger, F.; Reiter, R.; Tanasescu, R.; Zaffalon, P.-L.; Ziegler, A.; Müller, B.; Saxer, T.; Zumbuehl, A. *Nat. Nanotechnol.* **2012**, *7*, 536−543.
(16) Song, J.; Zhou, J.; Duan, H. *J. Am. Chem. Soc.* **2012**, *134*, 13458−13469.
(17) Kataoka, K.; Harada, A.; Nagasaki, Y. *Adv. Drug Delivery Rev.* **2001**, *47*, 113−131.
(18) Griset, A. P.; Walpole, J.; Liu, R.; Gaffey, A.; Colson, Y. L.; Grinstaff, M. W. *J. Am. Chem. Soc.* **2009**, *131*, 2469−2471.
(19) Tong, R.; Cheng, J. *Angew. Chem., Int. Ed.* **2008**, *47*, 4830−4834.
(20) Chen, J.; Chen, S.; Zhao, X.; Kuznetsova, L. V.; Wong, S. S.; Ojima, I. *J. Am. Chem. Soc.* **2008**, *130*, 16778−16785.
(21) Kim, B.; Han, G.; Toley, B. J.; Kim, C.-K.; Rotello, V. M.; Forbes, N. S. *Nat. Nanotechnol.* **2010**, *5*, 465−472.
(22) Wang, D.; Su, Y.; Jin, C.; Zhu, B.; Pang, Y.; Zhu, L.; Liu, J.; Tu, C.; Yan, D.; Zhu, X. *Biomacromolecules* **2011**, *12*, 1370−1379.
(23) Li, G.; Liu, J.; Pang, Y.; Wang, R.; Mao, L.; Yan, D.; Zhu, X.; Sun, J. *Biomacromolecules* **2011**, *12*, 2016−2026.
(24) Du, J.-Z.; Du, X.-J.; Mao, C.-Q.; Wang, J. *J. Am. Chem. Soc.* **2011**, *133*, 17560−17563.
(25) Singer, J. W.; Bhatt, R.; Tulinsky, J.; Buhler, K. R.; Heasley, E.; Klein, P.; Vries, P. D. *J. Controlled Release* **2001**, *74*, 243−247.
(26) Paranjpe, P. V.; Stein, S.; Sinko, P. J. *Anticancer Drugs* **2005**, *16*, 763−775.
(27) Khandare, J. J.; Chandna, P.; Wang, Y.; Pozharov, V. P.; Minko, T. *J. Pharmacol. Exp. Ther.* **2006**, *317*, 929−937.
(28) Greenwald, R. B.; Choe, Y. H.; McGuire, J.; Conover, C. D. *Adv. Drug Delivery Rev.* **2003**, *55*, 217−250.
(29) Yu, D.; Peng, P.; Dharap, S. S.; Wang, Y.; Mehlig, M.; Chandna, P.; Zhao, H.; Filpula, D.; Yang, K.; Borowski, V.; Borchard, G.; Zhang, Z.; Minko, T. *J. Controlled Release* **2005**, *110*, 90−102.
(30) Cheetham, A. G.; Zhang, P.; Lin, Y.-a.; Lock, L. L.; Cui, H. G. *J. Am. Chem. Soc.* **2013**, *135*, 2907−2910.
(31) Lock, L. L.; LaComb, M.; Schwarz, K.; Cheetham, A. G.; Lin, Y.-a.; Zhang, P.; Cui, H. G. *Faraday Discuss.* **2013**, *166*, 285−301.
(32) Shen, Y.; Jin, E.; Zhang, B.; Murphy, C. J.; Sui, M.; Zhao, J.; Wang, J.; Tang, J.; Fan, M.; Kirk, E. V.; Murdoch, W. J. *J. Am. Chem. Soc.* **2010**, *132*, 4259−4265.
(33) Husain, I.; Mohler, J. L.; Seigler, H. F.; Besterman, J. M. *Cancer Rev.* **1994**, *54*, 539−546.
(34) Pommier, Y. *Nat. Rev. Cancer* **2006**, *6*, 789−802.
(35) Maeda, H.; Seymour, L. W.; Miyamoto, Y. *Bioconjugate Chem.* **1992**, *3*, 351−362.
(36) Lyer, A. K.; Khaled, G.; Fang, J.; Maeda, H. *Drug Discovery Today* **2006**, *11*, 812−818.
(37) Mai, Y.; Zhou, Y.; Yan, D. *Macromolecules* **2005**, *38*, 8679−8686.
(38) Wang, Y.; Li, B.; Zhou, Y.; Lu, Z.; Yan, D. *Soft Matter* **2013**, *9*, 3293−3304.
(39) Lodge, T. P.; Rasdal, A.; Li, Z.; Hillmyer, M. A. *J. Am. Chem. Soc.* **2005**, *127*, 17608−17609.
(40) Kwon, G.; Naito, M.; Yokoyama, M.; Okano, T.; Sakurai, Y.; Kataoka, K. *Langmuir* **1993**, *9*, 945−949.
(41) Gottesman, M. M.; Fojo, T.; Bates, S. E. *Nat. Rev. Cancer* **2002**, *2*, 48−58.
(42) Shapira, A.; Livney, Y. D.; Broxterman, H. J.; Assaraf, Y. G. *Drug Resist. Updates* **2011**, *14*, 150−163.
(43) Chacanpatil, M. D.; Khdair, A.; Gerard, B.; Bachmeier, C.; Miller, D. W.; Shekhar, M. P. V.; Panyam, J. *Mol. Pharm.* **2007**, *4*, 730−738.
(44) Iversen, T.-G.; Skotland, T.; Sandvig, K. *Nano Today* **2011**, *6*, 176−185.
(45) Grütter, M. G. *Curr. Opin. Struct. Biol.* **2000**, *10*, 649−655.
(46) Lazebnik, Y.; Thornberry, N. A. *Science* **1998**, *281*, 1312−1316.
(47) Green, D. R. *Cell* **1998**, *94*, 695−698.
(48) Barreto, J.; O'Malley, W.; Kubeil, M.; Graham, B.; Stephan, H.; Spiccia, L. *Adv. Mater.* **2011**, *23*, H18−H40.
(49) Fox, M. E.; Guillaudeu, S.; Fréchet, J. M. J.; Jerger, K.; Macaraeg, N.; Szoka, F. C. *Mol. Pharm.* **2009**, *6*, 1562−1572.
(50) Wang, J.; Sun, X.; Mao, W.; Sun, W.; Tang, J.; Sui, M.; Shen, Y.; Gu, Z. *Adv. Mater.* **2013**, *25*, 3670−3676.
(51) Rajan, R. *Cancer* **2004**, *100*, 1365−1373.